

ZEEMAN CRATER'S ANOMALOUS MASSIF. A. C. Ruefer¹ and P. B. James¹, ¹Baylor University, Department of Geosciences, One Bear Place #97354, Waco, TX 76798 (Anna_Ruefer1@baylor.edu)

Introduction: The Moon's South Pole-Aitken (SPA) Basin is the largest and oldest feature on the lunar surface [1-3]. This basin records a massive impact event which played a significant role in the Moon's formation and may have produced an impact melt sea [4,5]. The SPA impact event produced enough energy to excavate the lunar mantle [3], yet spectral data reveals the occurrence of olivine in only a few locations [6], including the peak ring of Schrödinger crater and the central peak of Zeeman crater (Fig. 1), both of which lie at the southern floor of the SPA.

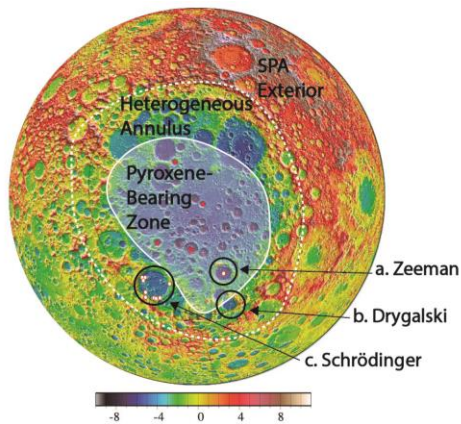


Figure 1: Topographic map of the SPA in km showing locations of craters in this study (black circles) with superimposed locations of spectrally-detected olivine (white dots) and pyroxene (red dots) reported by [6] and mineralogical regions outlined in [3].

Two prevailing mechanisms have been proposed to explain the anomalously feldspathic mineralogy of the SPA. In the first, the SPA stratigraphy formed as an impact melt sea differentiated into distinct layers of norite, pyroxenite, and dunite, with norite comprising the uppermost 12.5 km [7,12]. Modelling of Orientale basin suggests another mechanism, wherein the energy from the basin-forming impactor melts adjacent lunar crust which then flows into the basin, masking the underlying excavated ultramafic material [13].

This work investigates the origin of one particular topographic feature: a massif on the northwest rim of Zeeman crater that towers as much as 8 km above the crater floor. The origin, characteristics, and formation of this feature—and its significance in the broader context of the SPA basin—have been largely unexplored before now.

Spectral data guides further study, but is alone insufficient to address questions surrounding the origin of Zeeman's massif, where olivine has not been detect-

ed. Is this feature comprised of excavated mantle material thrown onto the crater rim? What mechanisms are responsible for its formation?

Density values distinguish rock composition, allowing further constraint on the formation of Zeeman crater. Here, we determine density across Zeeman, Schrödinger, and Drygalski crater for contextual evidence. Drygalski crater is located near Zeeman crater, on the farthest outlying extent of the SPA. Raised topography on this crater rim is likely comprised of remnant highland crust [8], thus providing comparison to Zeeman's massif.

Methods: We applied Nettleton's method to calculate bulk density at different locations of interest across the three craters. Nettleton's method determines the bulk density of a terrain through a simple linear regression between free air gravity and free air gravity expected from topography, from which slope yields our bulk density estimate within a standard error. High-resolution GRAIL gravity data was used for this analysis, with spherical harmonic bandpass limits of $l_1 = 200$ and $l_2 = 720$. For this waveband, an isostatic crust-mantle interface would contribute less than 1 mGal to the free air gravity anomaly. Therefore, we are confident that the gravity associated with this waveband is primarily produced by surface topography and the bulk density thereof. Finite amplitude from topography was calculated using LOLA topography data.

The bulk density is affected by the grain density of the rock as well as the porosity, so in order to infer the former we must quantify the latter. Spatio-spectral studies of the SPA basin have found a best-fit surface porosity of 26–33% and a best-fit depth scale of 2–3.5 km [9]. The depth sensitivity of the lunar gravity field is a function of the spherical harmonic degree, but an integration over the $l=200$ –700 waveband yields an effective porosity (ϕ_{eff}) of $10.8\% \pm 0.7\%$ for our bulk density measurements. Grain density can then be inferred by dividing the observed bulk density by a factor of $(1 - \phi_{\text{eff}})$.

Results: Grain density estimate results are plotted in Figure 2. Bulk density estimates for Zeeman crater's massif (1a) are $2.64 \pm 0.024 \text{ g cm}^{-3}$, compared to $2.75 \pm 0.084 \text{ g cm}^{-3}$ in the basin (3a). The massif estimate is slightly low compared to ~ 2.7 previously reported for the region around Zeeman [4]. Feature 1b on Drygalski crater yields a bulk density of $2.76 \pm 0.026 \text{ g cm}^{-3}$, and $2.58 \pm 0.037 \text{ g cm}^{-3}$ in the basin (3b). Schrödinger crater basin has a bulk density of $2.53 \pm 0.073 \text{ g cm}^{-3}$.

Discussion: The grain density expected for pure anorthosite is 2.75 g cm^{-3} , 2.95 g cm^{-3} for norite, 3.20 g cm^{-3} for pyroxenite, and 3.25 g cm^{-3} for dunite [12].

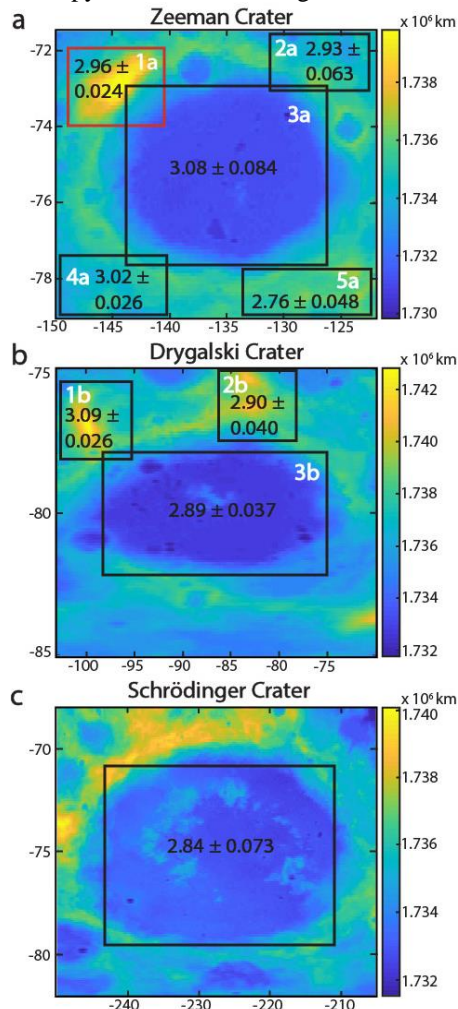


Figure 2: Topography maps showing grain density estimation within the masked area, indicated with black squares. Zeeman massif is shown within a red square.

1. The grain density for Drygalski crater basin (3b) is consistent with a feldspathic composition, while 1b falls within a more mafic range. 2b is consistent with a more noritic composition. These estimates challenge the previously assumed origin of this material (1-2b) as remnant highland crust.

2. Schrödinger crater's basin yields a density estimate lower than expected based on the spectral observation of olivine here. However, this crater is nearly twice as large as Zeeman or Drygalski, at roughly 320 meters in diameter [11]. The force of this impact likely produced fractures and porosity greater than accounted for in the SPA average. This highlights the significance of porosity assumptions in remote density estimations.

3. Inferred grain density for Zeeman crater's massif, consistent with norite, is low compared to $\sim 3.1 \text{ g}$

cm^{-3} estimated from Lunar Prospector data [4]. Taking the grain density for pure anorthosite (2.75 g cm^{-3}), we can place an upper bound of 42% on the volume fraction of ultramafic mineralogy in the massif. The basin interior has a slightly higher grain density, reflecting a greater abundance of ultramafic mineralogy consistent with spectral detections of olivine. Feature 5a yields the lowest density value in this study, consistent with pure anorthosite, yet lies hundreds of km from the proposed SPA exterior boundary.

Conclusions: We infer the impact melt sea hypothesis based on slightly higher average grain densities across the crater rims, consistent with an overlying noritic residuum. The crustal melt inflow hypothesis favors a lower density, feldspathic composition consistent with lunar highland anorthosite, but does not rule out the possibility for compositional mixing. Changes in density across these features highlights the complexity of the SPA. The effects of later crustal mixing from impact bombardment, or uncorrected variations in porosity may account for the variations we observe here.

What formed the anomalously high massif on Zeeman crater? While crater rims are typically elevated, this massif is too tall to have been formed solely by the Zeeman crater impact event. Density values eliminate the possibility of excavated mantle material, suggesting instead that the massif is autochthonous, comprised of the same material as the SPA floor. Alternatively, this massif may be a block of crust ejected during the SPA or another large impact, which became lodged in the SPA floor, prior to the Zeeman impact. In this case, a lower density, would be anticipated [10].

Acknowledgments: GRAIL and LOLA gravity data from the Planetary Data System (PDS) was used to generate the results in this study.

References: [1] Garrick-Bethel I. and Zuber M.T. (2009) *Icarus* 204, 399-408. [2] Lucey P.G. et al. (1998) *JGR* 103, 3701-3708. [3] Moriarty D.P. III and Pieters C.M. (2018) *JGR: Planets* 123, 729-747. [4] Wieczorek et al. (2012) *Science* 335, 1212-1215. [5] James P.B. et al. (2019) *GRL* 46, 5100-5106. [6] Yamamoto S. et al. (2010) *Icarus* 218, 331-344. [7] Vaughan W.M. and Head J.W. (2014) *PSS* 91, 101-106. [8] Campbell B.A. and Campbell D.B. (2006) *Icarus* 180, 1-7. [9] Besserer et al. (2014) *GRL* 41, 5771-5777. [10] Kiefer W.S. et al. (2012) *GRL* 39, L07201. [11] Petro N.E. and Pieters C.M. (2005) *JGR* 106, E06004. [12] Vaughan W.M. et al. (2013) *Icarus* 223, 749-765. [13] Johnson B.C. et al. (2017) *Science* 354, 441-444.